ELSEVIER

Thermochimica Acta 256 (1995) 33–46

thermochimica acta

A differential thermal analysis cell suitable for systems with vapour pressures exceeding ambient ☆

T. Grande *, S. Aasland, S. Julsrud [1]

Department of Inorganic Chemistry, Norwegian Institute of Technology, University of Trondheim, 7034 Trondheim, Norway

Abstract

In this paper we present a simple differential thermal analysis cell designed for measurements in corrosive and volatile salt systems with vapour pressures exceeding ambient pressure. The DTA assembly consists of a sealed platinum capsule, made from a cylindrical Pt tube, welded to a Pt/Pt10%Rh thermocouple for measuring the temperature of the sample. The differential temperature is obtained by using a reference Pt/Pt10%Rh thermocouple for recording the furnace temperature. A reference cell used in conventional DTA assemblies is not necessary in the present set-up due to the small total heat capacity of the DTA assembly relative to the heat capacity of the furnace environments. Our simple DTA cell has been applied successfully to determine the phase diagrams of several binary and ternary ZrF_4-based systems in the temperature region 200–1200°C. The triple point of pure ZrF_4, a compound which sublimes at ambient pressure, has also been obtained by the present method.

Keywords: DTA; Fluoride; Glass transition; Phase diagram

1. Introduction

Heavy metal fluoride glasses based on ZrF_4 have received considerable attention during the last two decades due to the promising optical properties of these vitreous

☆ Presented at the 14th Symposium on Thermal Analysis and Calorimetry, Oslo, Norway, 15–17 June 1994.

* Corresponding author.

[1] Present address: Norsk Hydro a.s., Research Centre, Porsgrunn, N-3901 Prosgrunn, Norway.

SSDI 0040-6031 (94) 02222-4

materials [1]. The physical properties of these ionic glasses are quite different from typical network oxide glasses, particularly the strong non-Arrhenius behaviour of their viscosity [1–3]. To get a better understanding of the interesting glass-forming properties of these fluoride melts, we undertook fundamental studies of their thermodynamic properties [4]. In this context we wanted to investigate the solid–liquid phase equilibria in these ZrF_4-based systems. An experimental challenge was, however, the high vapour pressures in melts with high contents of ZrF_4, combined with the corrosive nature of the melts and the tendency of metastable crystallization.

In conventional DTA cells the samples are contained in open crucibles, making the change of atmosphere and sample-container material easy. However, weight loss due to high vapour pressures is difficult to prevent in such cells, and they are therefore not suitable for high vapour pressure systems. DTA techniques for volatile molten salts have previously been developed [5], but the corrosive nature of ZrF_4 melts makes these techniques unsuitable. To be able to conduct phase investigations in ZrF_4-based systems we therefore found it necessary to develop a simple differential thermal analysis technique, designed for measurements in both corrosive and volatile molten salt systems. This new DTA technique is described and discussed in the present paper. Some examples of the application of the new technique and the results obtained are presented.

2. Description of the DTA cell

2.1. The differential thermal analysis cell

The experimental set-up of the DTA cell is given in Fig. 1. The sample is contained in a sealed cylindrical platinum ampoule (diameter 5 mm, length 20–40 mm, and Pt thickness 0.15 mm). The sealed end of the ampoule is welded to a Pt/Pt10%Rh thermocouple and attached to a 5 mm four-bore alumina (or mullite) tube using a platinum wire. The four-bore alumina tube shields the thermocouple wires connected to the ampoule as well as the wires of a Pt/Pt10%Rh reference thermocouple. The tip of the reference thermocouple is bent up along the alumina tube on the opposite side to the ampoule. Using this procedure both thermocouples are placed in the same horizontal plane, but are insulated from each other by the alumina tube.

The sample and reference thermocouples measure the temperature of the sample (T_s) and the furnace environments (T_r) during the temperature scans. Phase transitions in the samples are detected during heating and cooling by recording T_s and the differential temperature, $\Delta T = T_r - T_s$. Both T_s and ΔT are registered as a function of time using a Solartron 7151 multimeter (Solartron Instruments, England) connected to a strip chart recorder (Yokogawa 3021, Japan). The resulting differential temperature is therefore displayed as a function of time and not the sample temperature as in conventional DTA experiments.

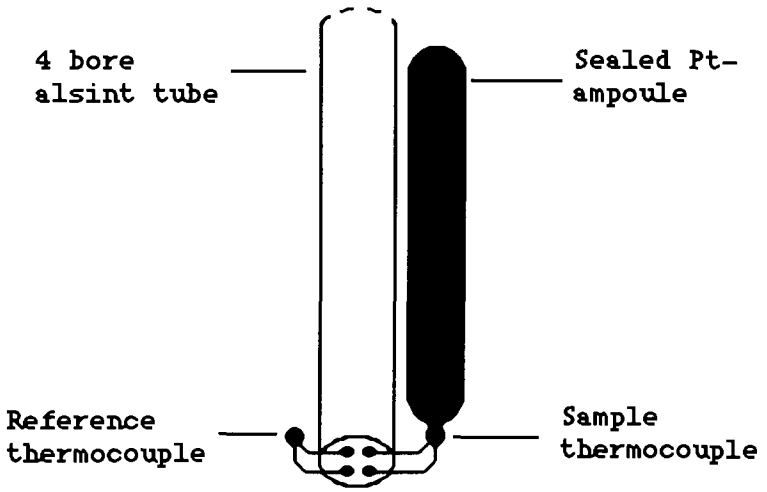

Fig. 1. The experimental set-up for the differential thermal analysis. The four-bore alumina tube shields and insulates the thermocouple wires from each other.

2.2. The Kanthal wound furnace

The differential thermal analysis was performed in a vertical Kanthal wound furnace (Kanthal wire A1, 12 mm diameter, 1.27 Ω m^{-1}) with a mullite furnace tube (65 mm outer diameter, 600 mm length) as shown in Fig. 2. To minimize the temperature gradient in the middle of the furnace, disc-shaped radiation shields, made from high alumina cement, are placed in the upper and lower part of the furnace tube. A temperature gradient of less than 4°C was obtained over the 10 cm hot zone between the radiation shields. The DTA assembly was placed in the furnace with the four-bore alumina tube extending to the outside of the furnace. The temperature gradient over the Pt capsule was less than 3°C (at constant furnace temperature), but the salt sample height in the ampoule was only 1.0–2.0 cm and the actual temperature gradient over the sample was therefore less than 2°C.

The four-bore alumina tube was fixed in the centre mullite tube using a cork on the outside of the furnace as shown in Fig. 2. Samples could then be introduced and changed easily.

The temperature in the furnace was controlled using a Eurotherm model 070 PID temperature controller (Eurotherm Ltd., England) with a Pt/Pt10%Rh thermocouple (see Fig. 2).

2.3. Preparation of the sealed Pt capsules with salt samples

The salt samples of about 1–2 g (mixtures of solid fluorides from BDH, England) were prepared in a glove box under N_2 atmosphere (<10 ppm O_2 and H_2O). The salts were transferred into a Pt cylinder (diameter 5 mm, cylinder-wall thickness 0.15 mm) which was sealed at one end by welding. The open end was

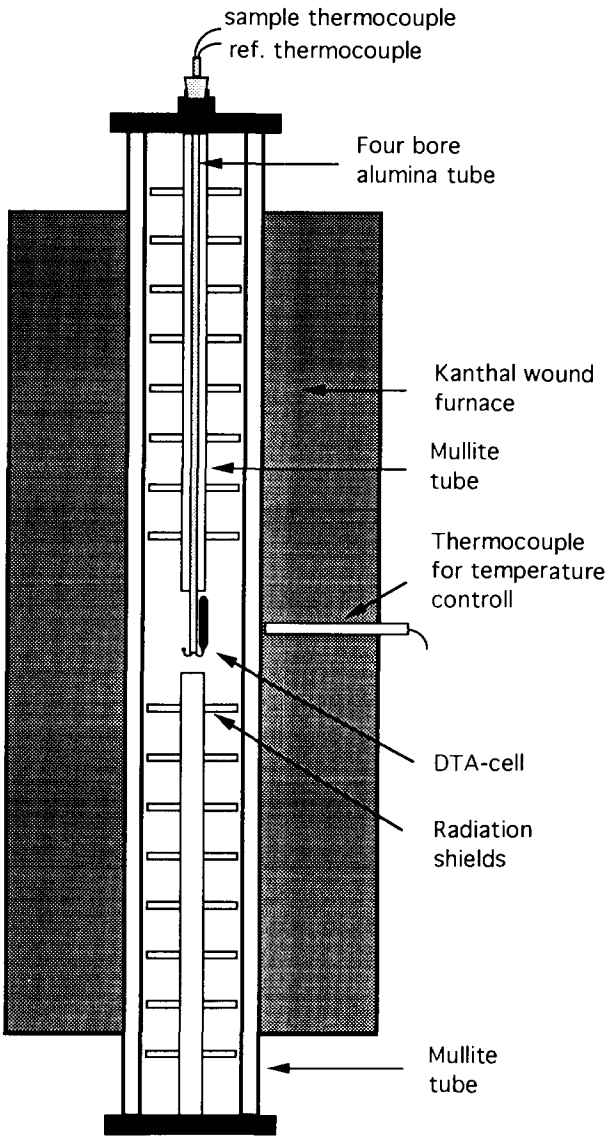

Fig. 2. Schematic diagram of the vertical Kanthal wound furnace with the DTA cell.

closed using a stop cock, and the Pt tube with the stop cock was transferred from the glove box, mounted on a vacuum line and evacuated to pressures $< 10^{-4}$ mbar. The tube walls were pinched together just above the level of the salts before welding, as shown in Fig. 3. The ampoule was finally welded to the sample thermocouple. The ampoule was water-cooled during the welding to avoid any evaporation of the salts. After analysis of each sample, the ampoule and the

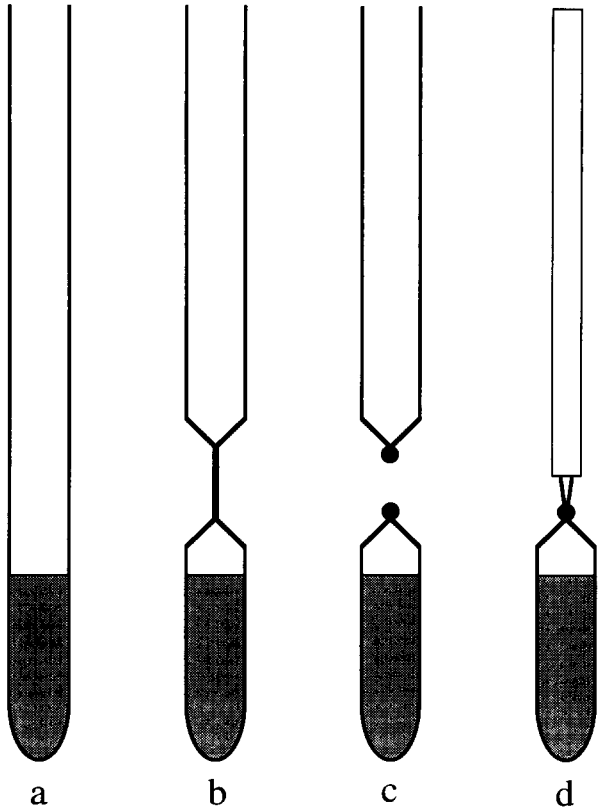

Fig. 3. The procedure for the sealing of the ampoule. (a) The Pt tube with salt sample in the bottom part of the tube. (b) The Pt tube walls pinched together above the sample. (c) The ampoule and the Pt tube after welding. (d) The ampoule welded to the thermocouple.

thermocouple were cut apart and another ampoule could be attached by the same procedure for analysis.

2.4. Temperature calibration

The sample thermocouple was calibrated in situ against the melting points of the pure components NaF, NaCl, AgCl, KNO_3 and the eutectic point in the system NaF–NaCl [6–10]. The ampoules used for the calibrations were prepared using the same procedure as for the salt mixtures.

The observed values for two different DTA cells and the literature data are given in Table 1, together with the reproducibility of the measurements. The uncertainty of each calibration point is estimated as the sum of the reproducibility of the measured value and the uncertainty of the literature value ($[\Sigma\,(SD)^2]^{1/2}$). Calibration curves for the two different DTA cells are shown in Fig. 4, where the deviation

Table 1
Data for the calibration of two DTA cells (IPTS-68). The literature values and the observed data are given in μV for a type-S thermocouple where the freezing point of pure water is the reference. The reproducibility of the measured data corresponds to the scatter in at least three parallels. The calibration factor ΔT is the difference between the literature and the observation. The uncertainty of each calibration point (ΔT) is estimated as the sum of the reproducibility of the measured and literature value ($[\Sigma (SD)^2]^{1/2}$)

Salt	T_{fus}/μV (°C) [Ref.]	DTA Cell 1		DTA Cell 2	
		T_{fus}/μV (°C) obs.	ΔT/μV	T_{fus}/μV (°C) obs.	ΔT/μV
KNO_3	2642 (334.6) [7]	2567 ± 20 (326.5)	75 ± 20		
AgCl	3811 ± 20 (457.0) [8]	3751 ± 4 (450.9)	60 ± 20	3760 ± 10 (451.8)	51 ± 22
NaCl–NaF	6068 ± 6 (680.4) [10]	6030 ± 3 (676.7)	38 ± 7	6032 ± 2 (676.9)	36 ± 6
NaCl	7362 ± 5 (801.6) [9]	7343 ± 2 (799.8)	19 ± 5	7337 ± 8 (799.3)	25 ± 9
NaF	9530 ± 5 (995.3) [11]	9528 ± 7 (995.1)	2 ± 9	9520 ± 7 (994.4)	10 ± 9

between the observed and literature values are given as a function of the observed temperature. T and ΔT are given in μV in the figures. The lines in the figures are the linear fits to the data. The equations for these two linear fits were used for temperature corrections of the measurements.

The accuracy of measured temperatures reported in the next section is estimated as the sum of the reproducibility of the measured temperature and the uncertainty of the calibration ($[\Sigma (SD)^2]^{1/2}$).

3. Examples of applications of the DTA cell

3.1. The melting point of ZrF_4

The triple point of ZrF_4 was determined to be 928 ± 2°C which is within the accuracy of the fusion temperature measured by drop calorimetry reported by McDonald et al. [11]. Two different modifications of ZrF_4 are reported in the literature [8], but we did not observe any phase transformation of ZrF_4(s). Our ZrF_4, which was purified by sublimation, was found to be β-ZrF_4 by XRD. We have only observed α-ZrF_4 in mixtures of AlF_3 and ZrF_4, and we believe that α-ZrF_4 is phase-stabilized by oxygen or aluminium contamination.

The vapour pressure of ZrF_4 at the triple point is 1.55 bar according to thermodynamic data [8]. We have been able to heat ZrF_4 about 30°C above its triple point which corresponds to a vapour pressure of 2.1 bar.

3.2. The phase diagram of the binary system BaF_2–ZrF_4

The melts in this system showed considerable supercooling, as expected for glass-forming systems. Only heating cycles were therefore used to establish the phase diagram. Due to metastable crystallization during cooling, annealing of the

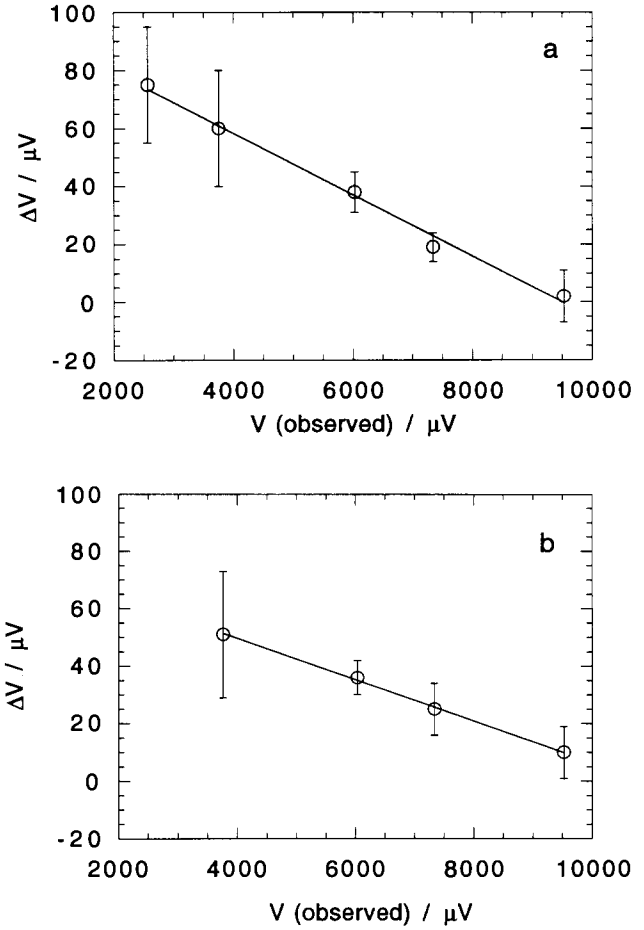

Fig. 4. Temperature calibration curves for: (a) DTA cell 1; and (b) DTA cell 2. The deviation between the measured and the literature values for the type-S thermocouples is displayed as a function of the observed voltage. The data in the two figures are given in Table 1. The displayed lines are linear fits to the observations.

samples at around 500°C was necessary to obtain equilibrium data. Metastable crystallization was due to the polymorphism of both $BaZr_2F_{10}$ and $BaZrF_6$ and the observed higher nucleation/crystallization rate of $BaZrF_6$ as compared to $BaZr_2F_{10}$ [12,13].

DTA curves for five different compositions in the system BaF_2–ZrF_4 are shown in Fig. 5. The compositions of the five samples are 28.9, 35.7, 46.9, 59.0 and 66.9 mol% BaF_2 respectively. Powder X-ray diffraction analysis was performed on samples quenched from different temperatures [12,13] to support the interpretation of the complex DTA curves.

The samples with 28.9 and 35.7 mol% BaF_2 shown in Fig. 5(a) and (b) are close to the composition of the binary compound $BaZr_2F_{10}$. $BaZr_2F_{10}$ melts congruently

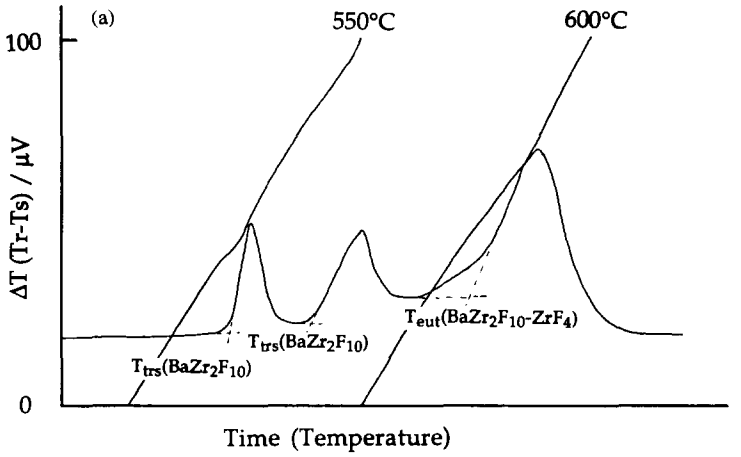
(a)
550°C
600°C
100
0
ΔT (Tr-Ts) / μV
$T_{trs}(BaZr_2F_{10})$
$T_{trs}(BaZr_2F_{10})$
$T_{eut}(BaZr_2F_{10}\text{-}ZrF_4)$
Time (Temperature)

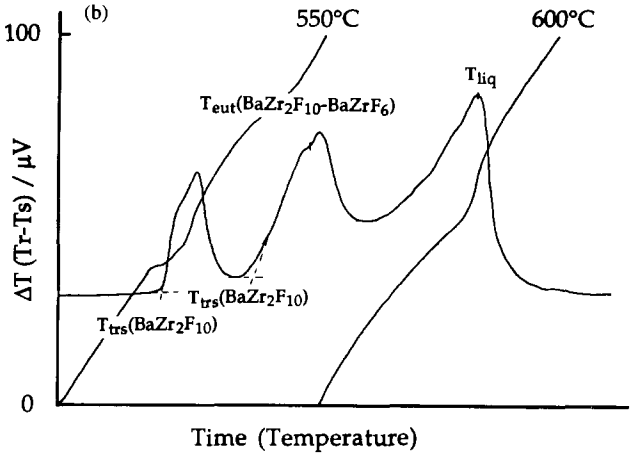
(b)
550°C
600°C
100
0
ΔT (Tr-Ts) / μV
T_{liq}
$T_{eut}(BaZr_2F_{10}\text{-}BaZrF_6)$
$T_{trs}(BaZr_2F_{10})$
$T_{trs}(BaZr_2F_{10})$
Time (Temperature)

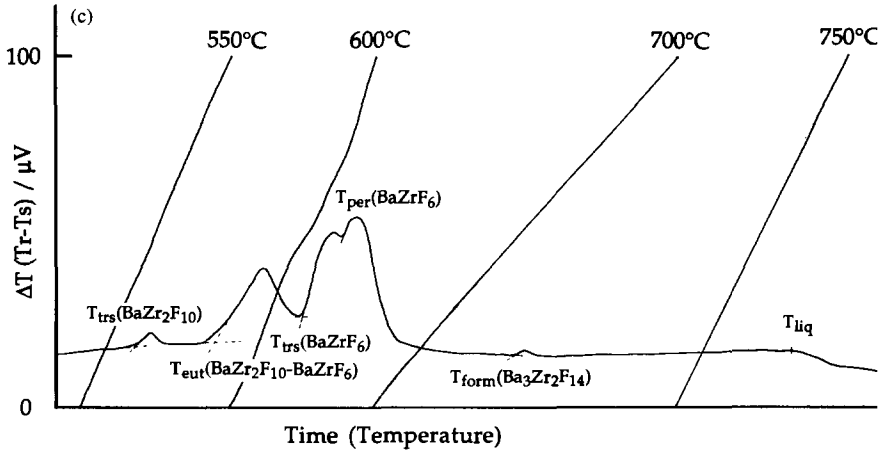
(c)
550°C
600°C
700°C
750°C
100
0
ΔT (Tr-Ts) / μV
$T_{per}(BaZrF_6)$
$T_{trs}(BaZr_2F_{10})$
$T_{trs}(BaZrF_6)$
$T_{eut}(BaZr_2F_{10}\text{-}BaZrF_6)$
$T_{form}(Ba_3Zr_2F_{14})$
T_{liq}
Time (Temperature)

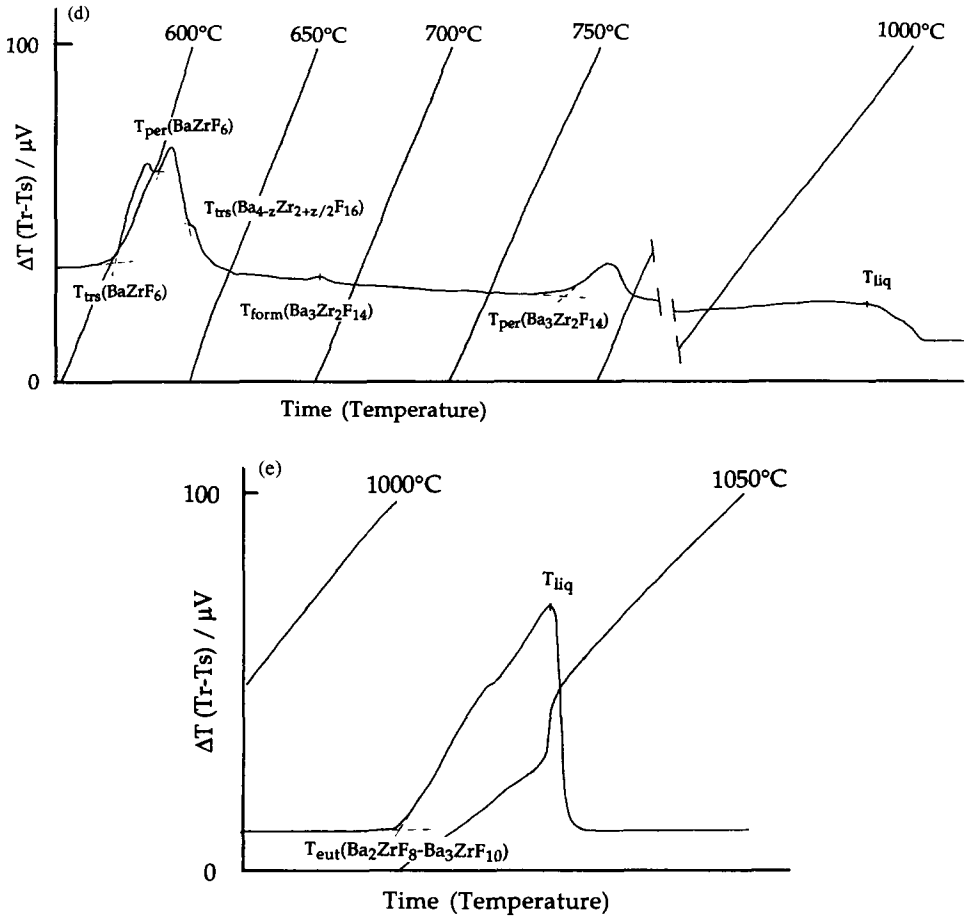

Fig. 5. DTA curves for five different compositions in the system BaF_2–ZrF_4. The compositions of (a) to (e) are 28.9, 35.7, 46.9, 59.0 and 66.9 mol% BaF_2 respectively. The heating rate of the experiments were 4, 4, 6–4, 6.5–3.5 and 3°C min^{-1} respectively. The interpretation of the endothermic effects are marked in the figures, where T_{trs} is the solid–solid phase transition temperature, T_{eut} the eutectic point, T_{per} the peritectic point, T_{form} the temperature of formation and T_{liq} the liquidus temperature. Note that the temperature interval between 770 and 950°C in figure (d) is not shown.

at 590 ± 2°C and undergoes two solid–solid phase transitions evident in both figures [12,13]. The first melt appears at different temperatures in these two samples due to two different eutectic temperatures on each side of $BaZr_2F_{10}$ at 569 ± 3 and 549 ± 1°C [13] (see Fig. 6).

The sample in Fig. 5(c) with 46.9 mol% BaF_2 is a mixture of the binary compounds $BaZrF_6$ and $BaZr_2F_{10}$ at sub-solidus temperatures. Six endothermic peaks due to phase transformations are evident in this curve: solid–solid phase transition of $BaZr_2F_{10}$, the eutectic point, the solid–solid phase transition of $BaZrF_6$, peritectic point of $BaZrF_6$, the formation of $Ba_3Zr_2F_{14}$, and finally the

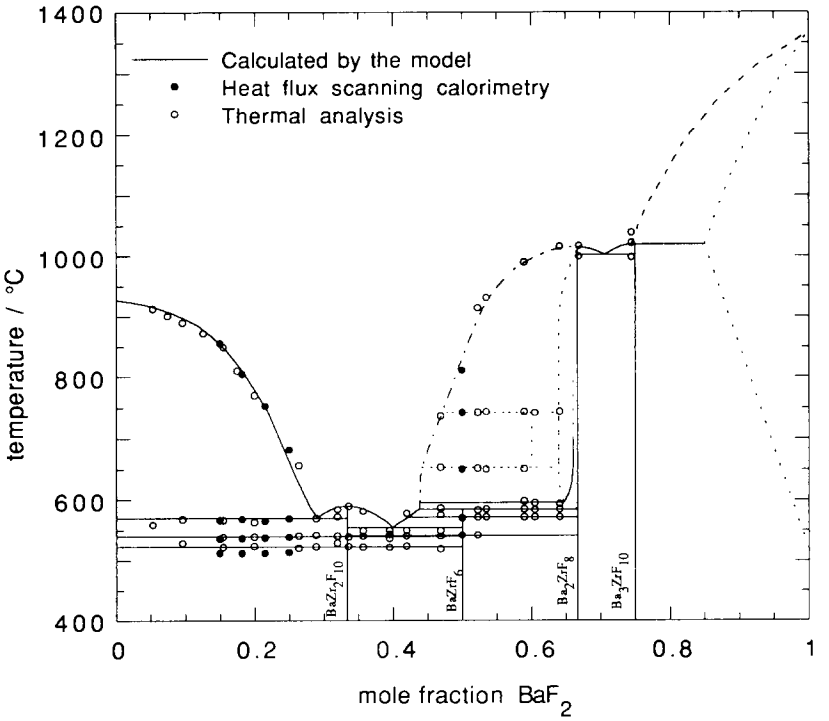

Fig. 6. The phase diagram of the binary system BaF_2–ZrF_4. The liquidus temperatures are calculated using a thermodynamic model for the system [13,14]. Some measurements by heat flux scanning calorimetry are also included in the figure [13].

liquidus temperature [13] (see Fig. 6). All these observations have been reproduced at least three times. We have not been able to confirm the existence of $Ba_3Zr_2F_{14}$ by XRD [13].

Six endothermic effects are also evident in Fig. 5(d) for the sample with 59.0 mol% BaF_2 which is a mixture of $BaZrF_6$ and Ba_2ZrF_8 at sub-solidus temperatures. The interpretation of the curves is as follows: solid–solid phase transition of $BaZrF_6$, peritectic point of $BaZrF_6$, solid–solid phase transition of $Ba_{4-z}Zr_{2+z/2}F_{16}$, formation of $Ba_3Zr_2F_{14}$, peritectic point of $Ba_3Zr_2F_{14}$, and finally the liquidus temperature [13] (see Fig. 6).

A DTA curve of a nearly pure sample of the congruently melting compound Ba_2ZrF_8 is shown in Fig. 5(e). Both the eutectic point between Ba_2ZrF_8 and Ba_3ZrF_{10} (see Fig. 6) and the fusion temperature are determined by the DTA curve.

The phase diagram of the system BaF_2–ZrF_4 based on DTA and XRD measurements is shown in Fig. 6 [13].

3.3. Glass transition and crystallization/remelting of a fluoride glass

A DTA curve for the heavy metal fluoride glass ZBLAN with composition in mol% (53 ZrF_4, 20 BaF_2, 4 LaF_3, 3 AlF_3, 20 NaF) is shown in Fig. 7. The sample

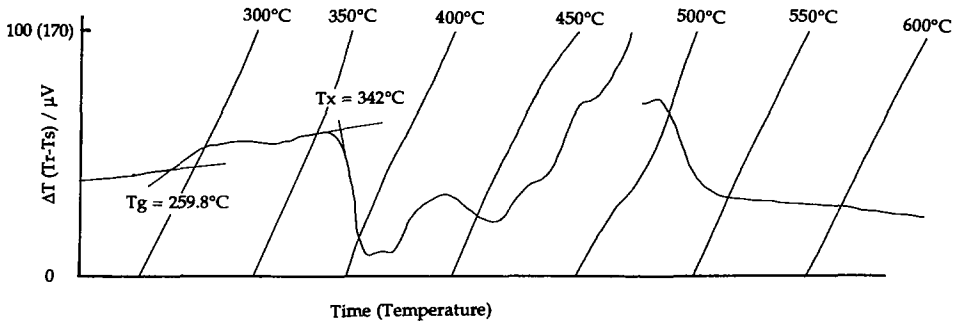

Fig. 7. DTA curve for the ZrF_4-based glass ZBLAN (in mol%: 53 ZrF_4, 20 BaF_2, 4 LaF_3, 3 AlF_3, 20 NaF). The glass transition temperature T_g and the onset temperature for the crystallization of the glass T_x are indicated. The heating rate of the scan is 14°C min^{-1}. Note that the scale for ΔT is changed from 100 to 170 μV at around 470°C.

used in the experiment was a powdered glass. The glass transition temperature as well as the crystallization of the glass is easily found by use of the present DTA cell. The complex shapes of the crystallization and the remelting peaks are due to the complex composition of the glass combined with the tendency for metastable crystallization.

3.4. Other systems

The DTA cell has been used for determination of several other phase diagrams including both binary and ternary ZrF_4-based systems [13–15].

4. Discussion

Factors influencing the DTA curves.

4.1. Furnace

Unlike in conventional DTA cells, the furnace atmosphere cannot influence the DTA curves in the present study because only sealed ampoules are used. The total heat content of the furnace environments is orders of magnitude larger than the heat content of the DTA cell. This is important for the performance of the cell as the influence on the furnace temperature of phase transitions in the sample is insignificant.

The heating rates we have obtained with the present furnace are in the region from about 1 to 15°C min^{-1}. Higher heating rates are not possible to obtain due to limited input power to the furnace. The practical minimum heating rate in the present cell is basically dependent on the performance of the temperature control of the furnace. Due to the relative large time constant of the furnace, the control

parameters have to be carefully tuned at low heating rates. We obtained the best signal-to-noise ratio by the most primitive temperature control, a constant power output. This will not, however, give a constant heating or cooling rate as shown in Fig. 5(d) where the heating rate changes continuously from about 6.5°C min^{-1} between 550 and 600°C to about 3.5°C min^{-1} between 950 and 1000°C. However, the effect of this small drift in the heating rate did not cause any problem in the analysis of the experimental curves.

The liquidus temperature of two- or multi-component samples involving large enthalpies of fusion or a flat liquidus line was found to decrease with decreasing heating rate. This is a well-known effect which is due to a temperature lag between the sample and the sample thermocouple [16]. For the samples which did show this dependence, we used the results obtained at about 1°C min^{-1} heating rate.

4.2. DTA cell

The critical factor for improving the sensitivity of the apparatus was to obtain a large thermal resistivity (slow heat transfer) between the two cells (sample and reference thermocouples) relative to the heat transfer between the DTA cell and the heat source (surface of the furnace tube). The four-bore alumina tube was sufficient as insulation. It prevented direct radiation between the sample and the reference, and also slowed down the horizontal convection. Convection will in any case be more important vertically in the furnace than horizontally. Heat transfer by conduction probably played a minor role.

The DTA cell was originally designed with a reference ampoule welded to the reference thermocouple to obtain a more stable baseline. However, we obtained satisfactory baselines in preliminary runs performed without a reference ampoule, and we therefore decided to carry out the DTA experiments without any reference ampoule. A reasonable approximation for this configuration is that the heat capacity of the reference cell is negligible ($C_{p,r} \approx 0$). By application of the theory for differential thermal analysis described by Gray [17], the following expression can be given for the instantaneous rate of heat generation of the sample

$$R\left(\frac{dH}{dt}\right) = (T_s - T_r) + RC_{p,s}\left(\frac{dT_r}{dt}\right) + RC_{p,s}\left(\frac{d(T_s - T_r)}{dt}\right) \quad (1)$$

where R is the thermal resistivity of both cells. This equation is valid for our DTA cell if the assumption that R is equal for both the sample and the reference is reasonable. One should have in mind the change in sensitivity of the cell with temperature and heating rate. The thermal resistivity R decreases with increasing temperature which reduces the sensitivity at high temperatures. The form of Eq. (1) shows that we can interpret our curves by the same procedures as for conventional DTA cells.

In the temperature range from 200 to 1200°C, relevant for our studies, the mechanism of the heat transfer is dominated by convection in the lower temperature range, while radiation is the most important factor at high temperatures. This change causes a decrease in the thermal resistivity between the heat source and the

cell (R in Eq. (1)) with increasing temperature. Taking this into account one would expect a drift in the baseline as the factor $R(C_{p,s} - C_{p,r})\,dT_r/dt$ in Eq. (1) depends on R. Such a drift in the baseline is also evident in the curves given in Fig. 5(c) and (d). However, we cannot attribute the drift in the baseline entirely to changes in R as long as the heating rate was not constant. The baseline also decreases with decreasing heat rate (dT_r/dt) as shown by Eq. (1).

The platinum ampoule functioned satisfactory as the sample holder in the present cell, excluding problems with reduced resolution due to sample holder material and geometry. Good thermal contact between the sample and the thermocouple was assured by the welded joint between the thermocouple and the ampoule. The sensitivity of the cell was only limited due to the platinum metal, but Pt is a good thermal conductor and the sensitivity was therefore good.

The main disadvantage of the present method is the location of the thermocouple in the sample which decreases the resolution. A larger diameter of the ampoule would reduce the average distance at a constant sample size. Our choice to work with ampoules of 5 mm diameter was due to the convenience of preparing ampoules with this diameter.

4.3. Sample characteristics

The sample mass in the present cell is typically 1–2 g. We chose this amount of salt to obtain satisfactory accuracy of the composition of the samples (restricted by the balance in the glove box). This was more than sufficient material to obtain a good signal-to-noise ratio, and the sample mass could have been reduced by a factor of 10 without losing information. The sample mass can be increased by increasing the diameter of the ampoule if necessary. However, one should have in mind the distance between the sample and the thermocouple if much larger samples are needed/used.

Problems with particle size, packing density, thermal resistivity between sample grains and container, and the degree of crystallinity of the samples were minimized in the present set-up due to the possibility of melting the entire sample before the analysis. Samples with high homogeneity, low porosity and good thermal contact to the Pt wall were obtained by melting the samples above the liquidus temperature followed by quenching below the solidus temperature, and subsequent annealing to avoid the presence of metastable phases.

4.4. Temperature calibration

Metal standards traditionally used for temperature calibration were not used as they would have formed alloys with platinum. Salt samples were preferred due to the relative good match in density, thermal conductivity and heat capacity with the examined samples. Contamination of the thermocouples with time was checked regularly without any observations of drift in the voltage of the DTA cell. We showed in separate experiments that the calibrations were not dependent on the heating rate.

5. Conclusions

A simple differential thermal analysis set-up designed for measurements on corrosive and volatile salt systems with vapour pressures exceeding ambient has been developed. The DTA assembly has been applied successfully to determine the phase diagrams of several binary and ternary ZrF_4-based systems in the temperature region 200–1200°C. The triple point of pure ZrF_4, a compound which sublimes under ambient pressure, has also been determined using the present method. The method was sensitive enough to detect the glass transition temperature of a ZrF_4-based glass.

Acknowledgements

Financial support from the Royal Norwegian Council for Scientific and Industrial Research (NTNF) and the Norwegian Research Council for Science and Humanities (NAVF) is gratefully acknowledged.

References

[1] J. Lucas and J.L. Adam, Glastech. Ber., 62 (1989) 422.
[2] W.C. Hasz and C.T. Moynihan, J. Non-Cryst. Solids, 140 (1992) 285.
[3] T. Grande, H.A. Øye and S. Julsrud, J. Non-Cryst. Solids, 161 (1992) 152.
[4] T. Grande and S. Julsrud, Mater. Sci. Forum, 32 (1988) 643.
[5] L.O. Gilpatrick, S. Cantor and C.J. Barton, in R.F. Schwenker and P.D. Garn (Eds.), Thermal Analysis, Academic Press, New York, 1969, p. 85.
[6] I. Barin, Thermochemical Data of Pure Substances, VCH, Germany, 1989.
[7] R. Blachnik and G. Kudermann, Z. Naturforsch., 28 (1973) 1.
[8] JANAF Thermochemical Tables, J. Phys. Chem. Ref. Data, 14 (1985).
[9] C.E. Johnson and E.J. Hathaway, J. Electrochem. Soc., 118 (1971) 631.
[10] S. Julsrud, Dr. Thesis, Norwegian Institute of Technology, University of Trondheim, 1983.
[11] R.A. McDonald, G.C. Sinke and D.R. Stull, J. Chem. Eng. Data, 7 (1962) 83.
[12] T. Grande, S. Aasland and S. Julsrud, J. Non-Cryst. Solids, 140 (1992) 73.
[13] T. Grande, Dr. Thesis, Norwegian Institute of Technology, University of Trondheim, 1992.
[14] T. Grande, S. Aasland and S. Julsrud, J. Non-Cryst. Solids, 161 (1993) 86.
[15] S. Aasland, T. Grande and S. Julsrud, J. Non-Cryst. Solids, 140 (1992) 69.
[16] W.W. Wendlandt, Thermal Analysis, John Wiley and Sons, New York, 1986, p. 230.
[17] A.P. Gray, in R.F. Porter and J.M. Johnson (Eds.), Analytical Calorimetry, Plenum Press, New York, 1968, p. 209.